The receptor tyrosine kinase EPHB6 regulates catecholamine exocytosis in adrenal gland chromaffin cells

Received for publication, February 28, 2020, and in revised form, April 20, 2020 Published, Papers in Press, April 22, 2020, DOI 10.1074/jbc.RA120.013251

Wei Shi[1,‡], **Bei Ye**[1,2,‡], **Marion Rame**[3], **Yujia Wang**[2], **Dominique Cioca**[4], **Sophie Reibel**[4], **Junzheng Peng**[1], **Shijie Qi**[1], **Nicolas Vitale**[3,*], **Hongyu Luo**[1,*], **and Jiangping Wu**[1,5,*]

From the [1]*Research Centre, Centre hospitalier de l'Université de Montréal (CRCHUM), Montreal, Quebec, Canada,* [2]*Children's Hospital, Zhejiang University School of Medicine, Hangzhou, Zhejiang, China,* [3]*Institut des Neurosciences Cellulaires et Intégratives, UPR-3212 Centre National de la Recherche Scientifique and Université de Strasbourg, Strasbourg, France,* [4]*Chronobiotron UMS 3415, Strasbourg, France, and* [5]*Nephrology Department, CHUM, Montreal, Quebec, Canada*

Edited by Enrique M. De La Cruz

The erythropoietin-producing human hepatocellular receptor EPH receptor B6 (EPHB6) is a receptor tyrosine kinase that has been shown previously to control catecholamine synthesis in the adrenal gland chromaffin cells (AGCCs) in a testosterone-dependent fashion. EPHB6 also has a role in regulating blood pressure, but several facets of this regulation remain unclear. Using amperometry recordings, we now found that catecholamine secretion by AGCCs is compromised in the absence of EPHB6. AGCCs from male knockout (KO) mice displayed reduced cortical F-actin disassembly, accompanied by decreased catecholamine secretion through exocytosis. This phenotype was not observed in AGCCs from female KO mice, suggesting that testosterone, but not estrogen, contributes to this phenotype. Of note, reverse signaling from EPHB6 to ephrin B1 (EFNB1) and a 7-amino acid-long segment in the EFNB1 intracellular tail were essential for the regulation of catecholamine secretion. Further downstream, the Ras homolog family member A (RHOA) and FYN proto-oncogene Src family tyrosine kinase (FYN)–proto-oncogene c-ABL–microtubule-associated monooxygenase calponin and LIM domain containing 1 (MICAL-1) pathways mediated the signaling from EFNB1 to the defective F-actin disassembly. We discuss the implications of EPHB6's effect on catecholamine exocytosis and secretion for blood pressure regulation.

Erythropoietin-producing human hepatocellular receptors (EPH) are the largest family of receptor tyrosine kinases. Their ligands are ephrins (EFN), which are also cell membrane molecules (1). EPHs are classified into A and B subfamilies based on their sequence homology. EFNs are also categorized into A and B subfamilies, based on the way they anchor on the cell membrane. EFNAs attach to the cell membrane by a glycosylphosphatidylinositol linkage, and they are without intracellular tails. EFNBs are transmembrane molecules. EPH and EFN interact promiscuously, but generally speaking, EPHAs preferably interact with EFNAs, and EFPBs with EFNBs (2). EPHB6 is an inactive receptor tyrosine kinase due to a mutation in its kinase domain. EPH kinases and EFNs have profound and diverse functions in physiology and pathophysiology in almost all the systems in our bodies. Their functions were first reported in the nervous system (2, 3). Subsequently, EPHs and EFNs were found to be essential in intestinal epithelial cell maturation (4), bone metabolism (5), angiogenesis (6), immune responses (7), insulin secretion (8), kidney glomerular filtration (9), chemotaxis (10), and homeostasis of vestibular endolymph fluid in the inner ear (11), etc.

Our recent work revealed that EPHs/EFNs are critical in controlling blood pressure, according to mouse models and human genetic studies (12–21). The target tissues of such EPHs/EFN functions are vascular smooth muscles and adrenal gland chromaffin cells (AGCCs). In male but not female EPHB6 gene knockout (KO) mice, their 24-h urine catecholamine (CAT) levels are reduced, but castration reverts the levels to a normal range (12). Using isolated AGCCs, we have shown that in the absence of EPHB6, the acetylcholine (ACh)-triggered Ca^{2+} influx of the KO AGCCs is compromised. This is in part caused by an increase in big potassium channel (BK) current, causing premature closure of voltage-gated calcium channels, leading to decreased Ca^{2+} influx (19).

Ca^{2+} flux is a secondary messenger in excitable cells and influences multiple downstream events. In AGCCs, it controls long-term CAT synthesis as well as CAT exocytosis (22, 23). Accordingly, AGCCs from male EPHB6 KO mice have a lower CAT content, caused by a reduced level of tyrosine hydroxylase (24), the rate-limiting enzyme of CAT synthesis. In this study, we assessed whether EPHB6 KO affected CAT exocytosis and studied underlying mechanisms.

Results

Reduced CAT exocytosis in male KO AGCCs

Our previous study has shown a reduction of 24-h urine CAT levels in EPHB6 KO male but not female mice. To prove that such reduction was due to decreased CAT secretion by AGCCs, we conducted amperometry to assess CAT release by individual AGCCs. Typical amperometry traces of AGCCs from male KO and wildtype (WT) mice are shown in Fig. 1*A*. Compared with WT counterparts, KO AGCCs from male mice presented a significantly reduced spike number per cell within the first 2 s of ACh stimulation (Fig. 1*B*) and within 60 s (Fig. 1*C*). The maximal spike height (I_{max}, Fig. 1*D*) and charge per peak (Q, Fig. 1*E*) of the KO AGCCs were also reduced, although the spike width

This article contains supporting information.
‡ These authors contributed equally to this work.
* For correspondence: Dr. Jiangping Wu, jianping.wu@umontreal.ca; Dr. Hongyu Luo, hongyu.luo@umontreal.ca; Dr. Nicolas Vitale, vitalen@inci-cnrs.unistra.fr.

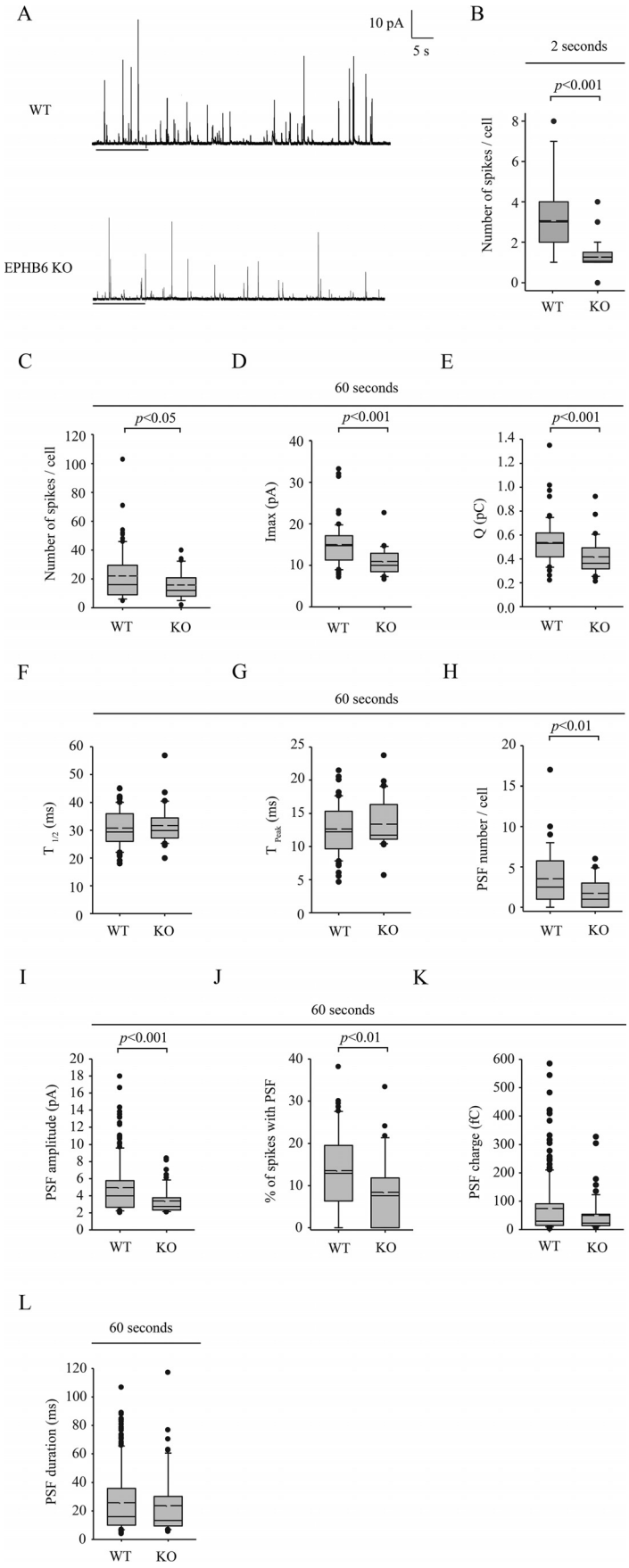
A
10 pA
5 s
WT
EPHB6 KO
B
2 seconds
p<0.001
Number of spikes / cell
WT
KO
C
D
E
60 seconds
p<0.05
Number of spikes / cell
p<0.001
Imax (pA)
p<0.001
Q (pC)
F
G
H
60 seconds
T 1/2 (ms)
T Peak (ms)
p<0.01
PSF number / cell
I
J
K
60 seconds
p<0.001
PSF amplitude (pA)
p<0.01
% of spikes with PSF
PSF charge (fC)
L
60 seconds
PSF duration (ms)

at half-height ($T_{½}$, Fig. 1*F*) and the time to reach the peak (T_{peak}, Fig. 1*G*) were not significantly different from their WT counterparts.

Analysis of the pre-spike feet (PSF) showed that the number of PSF per cell (Fig. 1*H*), the PSF amplitude (Fig. 1*I*), and the percentage of spikes with PSF (Fig. 1*K*) were all significantly reduced in AGCCs from male KO mice, compared with their WT counterparts. However, the PSF charge (Fig. 1*K*) and duration (Fig. 1*L*) were comparable between KO and WT AGCCs from male mice. Of note, all these amperometry parameters, including the number of spikes per cell were not significantly different in AGCCs from female KO and WT mice (Fig. S1).

Compromised cortical filamentous actin (F-actin) network disassembly in KO AGCCs upon ACh stimulation

We next examined the cortical F-actin morphology in AGCCs after nicotine stimulation using confocal microscopy. Typical micrographs of continuous and disassembled cortical F-actin in resting and activated WT AGCCs (40 s after nicotine stimulation) are shown in Fig. 2*A*. The percentages of cells with disassembled F-actin ring in the resting KO and WT AGCCs cells are similar (Fig. 2*B*). When examined between 20 and 60 s after nicotine stimulation, KO AGCCs showed a consistently lower percentage of cells with disassembled cortical F-actin (Fig. 2*B*). However, after castration, the KO AGCCs reverted to the WT morphology as the percentage of cells with disassembled F-actin increased to a level similar to that of WT AGCCs (Fig. 2*B*). Castration did not affect the F-actin disassembly in WT AGCCs (Fig. 2*C*). F-actin disassembly in AGCCs from female KO and WT mice was also similar (Fig. 2*D*). Altogether these results suggest that EPHB6 deletion and testosterone are both indispensable for the compromised F-actin disassembly in AGCCs from male KO mice.

We further elucidated how sex hormones in concert with EPHB6 regulated F-actin disassembly. When AGCCs from female KO mice were treated shortly for 15 min with cell-impermeable BSA-conjugated testosterone, their F-actin disassembly was compromised (Fig. 2*E*). BSA-conjugated testosterone had no effect on AGCCs from WT females (Fig. 2*F*), excluding the possibility that testosterone alone affected the F-actin disassembly. In contrast, when estrogen was added to the culture of AGCCs from male WT (Fig. 2*G*) or KO (Fig. 2*H*) mice, it manifested no significant effect on the F-actin disassembly.

To prove that the reduced F-actin disassembly in KO cells due to cell-impermeable testosterone did have a functional consequence in terms of CAT secretion, we treated female AGCCs with BSA-conjugated testosterone. Such treatment indeed significantly reduced noradrenaline secretion by KO but not WT AGCCs (Fig. 2*I*). Altogether, these data indicate that the observed compromised F-actin disassembly in AGCCs from male KO mice is due to EPHB6 deletion in concert with the nongenomic effect of testosterone, whereas the absence of estrogen does not play a role in this matter. Furthermore, such F-actin disassembly appears functionally associated with CAT secretion.

EPHB6 reverse signaling through EFNB1 is essential in regulating CAT exocytosis in AGCC

EPHB6 and its ligands (EFNBs) are capable of bidirectional signaling. To discern these two types of signaling related to CAT exocytosis of AGCCs, we employed solid-phase EPHB6 (EPHB6-FC– coated wells) and solid-phase anti-EPHB6 Ab (anti-EPHB6 Ab-coated wells) to stimulate tsAM5NE cells, which are derived from normal AGCCs (25). In the adrenal gland medullae, there are two types of chromaffin cells containing either epinephrine (EPI) or norepinephrine (NE) (26). They secret EPI or NE, respectively (27). tsAM5NE cells are NE-secreting AGCCs (25); their NE secretion was used as a readout.

As shown in Fig. 3*A*, solid-phase EPHB6 significantly augmented ACh-triggered NE release by AGCCs, whereas solid-phase anti-EPHB6 Ab had no such effect. Their respective proteins control normal human IgG (the Fc part of EPHB6-Fc was of human IgG origin) or normal mouse IgG did not impact on the NE release. This result indicated that the reverse signaling from EPHB6 to EFNBs was responsible for regulating NE exocytosis in AGCCs.

To identify which EFNB was mediating such reverse signaling, we placed Ab against two major EPHB6 ligands, *i.e.* EFNB1 and EFNB2, on the solid-phase, and used them to stimulate tsAM5NE cells. Anti-EFNB1 but not anti-EFNB2 Ab drastically augmented ACh-stimulated NE secretion (Fig. 3*B*), suggesting that the major reverse signaling was mediated by EFNB1.

EFNBs have no enzymatic activity, and their reverse signaling depends on the association of other signaling molecules with their short intracellular sequences. In the intracellular sequence of EFNB1, there are 5 tyrosine residues and a PDZ-binding domain at its C terminus (Fig. 3*C*). We constructed lentiviruses expressing full-length EFNB1 and various deletion mutants of the EFNB1 intracellular sequence (Fig. 3*C*). tsAM5NE cells were infected with these viruses. By adjusting virus concentrations, the tsAM5NE cell-surface overexpression of different EFNB1 mutants was titrated to a similar level according to flow cytometry (Fig. S2). The method of flow cytometry was described in the supplementary methods in supplementary Information. tsAM5NE cells overexpressing the full-length EFNB1 increased NE secretion significantly, com-

Figure 1. Reduced CAT release from KO AGCCs from KO and WT male mice according to amperometry recording. AGCCs were isolated from three KO and three WT male mice, and their nicotine-stimulated CAT release was registered by amperometry. Typical traces of amperometry are shown in *A*. Box bar graphs (*B–L*) show the medium (*solid horizontal line in the box*), mean (*dashed horizontal line in the box*), the 75th percentile (*upper part of the box*), 25th percentile (*lower part of the box*), 95th percentile (*upper whisker*), 5th percentile (*lower whisker*), and outliners (*dots* beyond the 95th and 5th percentiles) of each parameter. The Mann-Whitney Rank Sum tests were conducted for statistical analysis due to failed normality tests of the data. Significant *p* values are shown. The number of spikes per cell observed in the 2- (*B*) or 60-s (*C*) period after nicotine stimulation, the spike peak height (I_{max}) (*D*), the charge of the spikes (*Q*) (*E*), the half-time to reach the spike peak ($T_{½}$) (*F*), the time to reach the peak (T_{peak})(*G*), the number of PSF observed per cell (*H*), the PSF amplitude (*I*), the percentage of spikes with PSF (*J*), the PSF charge (fC) (*K*), and the PSF duration (*L*) are illustrated. For *B–G*, 89 WT cells and 35 KO cells were analyzed; for *H* and *J*, 60 WT cells and 30 KO cells; *I* and *K*, 212 PSF of WT cells, and 52 PSF of KO cells. The values in *B*, *C*, and *H* were averaged per cell for the duration indicated. The values in the remaining panels were calculated according to all events that occurred in all the cells tested during the 60-s recording period.

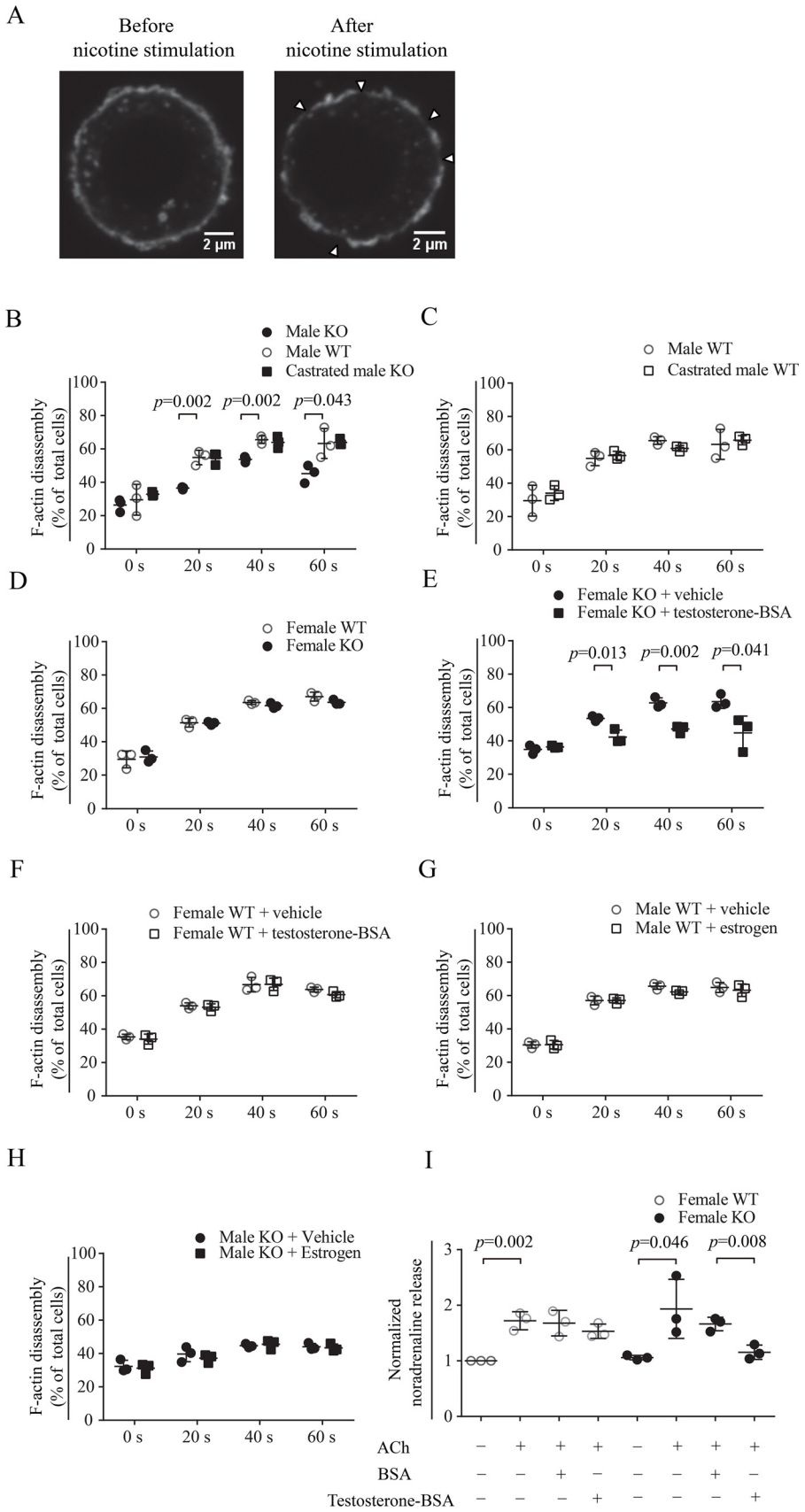
A
Before nicotine stimulation
After nicotine stimulation
2 μm
2 μm
B
Male KO
Male WT
Castrated male KO
p=0.002
p=0.002
p=0.043
F-actin disassembly (% of total cells)
0 s
20 s
40 s
60 s
C
Male WT
Castrated male WT
D
Female WT
Female KO
E
Female KO + vehicle
Female KO + testosterone-BSA
p=0.013
p=0.002
p=0.041
F
Female WT + vehicle
Female WT + testosterone-BSA
G
Male WT + vehicle
Male WT + estrogen
H
Male KO + Vehicle
Male KO + Estrogen
I
Female WT
Female KO
p=0.002
p=0.046
p=0.008
Normalized noradrenaline release
ACh
BSA
Testosterone-BSA

pared with the empty virus-infected cells (both of them were cultured in anti-EFNB1 Ab-coated wells) (Fig. 3*D*). The cells with full-length EFNB1 overexpression and cultured in anti-EFNB1 AB-coated wells also had significantly increased NE secretion compared with the same kinds of cells cultured in wells coated with control IgG (*i.e.* without reverse signaling via EFNB1) (Fig. 3*D*). These controls validated the assay system as one being able to detect reverse signaling by overexpressed EFNB1 over the endogenous EFNB1 on the tsMA5NE cell surface. EFNB1-Δ2Y (the deletion of the last 16 aa of the C terminus including the PDZ-binding domain and two tyrosine residues, Tyr-342 and Tyr-343) was equally potent as the full-length EFNB1. The further deletion of 7 aa, including tyrosine residues Tyr-323 and Tyr-328 (EFNB1-Δ4Y), significantly reduced the potency of the mutant to stimulate NE secretion. The additional deletion of 11 aa containing the remaining tyrosine residues Tyr-312 and Tyr-316 (EFNB1-Δ6Y) did not result in a further decrease of the potency. These results suggested that the critical sequence mediating EFNB1 reverse signaling in mouse AGCCs in terms of controlling CAT secretion resided within the 7-aa intracellular sequence from aa 322 to 328, containing Tyr-323 and Tyr-328.

It has been established that EFNB1 reverse signaling depends on several RHO family G-proteins (13, 28–30). We found that RHOA activity after nicotine stimulation in AGCCs from male KO was increased compared with their WT counterparts (Fig. 3*E*). This is compatible with prior knowledge that heightened RHOA activity increases actin polymerization (31) and hence reduces overall F-actin disassembly as a result. When AGCCs from male WT mice were treated with RHOA inhibitor Rhosin, no effect on F-actin disassembly was observed (Fig. 3*F*). However, such inhibition reverted the decreased F-actin disassembly in the KO cells to a level similar to that of the WT counterparts (Fig. 3*F*). This result indicated that the increased RHOA activity in the KO AGCCs contributed to the diminished F-actin disassembly.

The FYN/c-ABL/MICAL-1 pathway conducted signaling from EPHB6 to F-actin disassembly

FYN was previously reported to interact with EFNB1 (32) and therefore is a possible downstream signaling molecule mediating EPHB6 reverse signaling in AGCCs concerning their function in CAT secretion. The SRC-family tyrosine kinase FYN was activated (based on its Tyr-420 phosphorylation) within 5–10 min of nicotine stimulation in AGCCs of WT male mice (Fig. 4*A*). Such phosphorylation was compromised in the KO AGCCs, whereas the total FYN protein remained unchanged (Fig. 4*A*). The tyrosine kinase c-ABL is a substrate of FYN kinase (33). Its phosphorylation, which is needed for its activation (33), was diminished, as expected, in AGCCs from male KO mice (Fig. 4*B*). In this experiment, total phosphoprotein was immunoprecipitated, followed by anti-c-ABL Ab blotting. We previously demonstrated that the phosphorylation of ELK1 was not influenced by EPHB6 KO in AGCCs (24). Fig. 4*B* showed that ELK1 phosphorylation was similar in all the precipitated samples and was used as a loading and immunoprecipitation efficiency control. Furthermore, the total protein of c-ABL in the KO and WT AGCCs was similar (Fig. 4*C*).

MICAL-1 is a substrate of the c-ABL kinase (34) and is an F-actin-monooxygenase, which oxidizes methionine residues of actin (35). It is essential in promoting the depolymerization of F-actin (35), and its phosphorylation is necessary for its activity (34). Although total MICAL-1 protein levels in WT and KO AGCCs were similar in resting and 10-min nicotine-stimulated cells (Fig. 5*A*), MICAL-1 phosphorylation was significantly increased in stimulated male WT AGCCs (Fig. 5*B*). This augmentation was compromised in the KO AGCCs (Fig. 5*B*). FYN inhibitor PP2 suppressed the up-regulation of nicotine-stimulated MICAL-1 phosphorylation in the male WT AGCCs but did not affect the KO counterparts (Fig. 5*B*), supporting a model in which FYN acted downstream of EPHB6, and this activity appeared upstream of MICAL-1 phosphorylation. When the male WT AGCCs were treated with Imatinib, a c-ABL inhibitor, their MICAL-1 phosphorylation up-regulation upon nicotine stimulation was compromised (Fig. 5*C*). On the other hand, imatinib had no such effect on KO counterparts, suggesting that c-ABL activity was downstream of EPHB6 and upstream of MICAL-1 phosphorylation in these cells. ELK1 phosphorylation was again employed as an internal control for the efficiency of immunoprecipitation and loading in this experiment.

To assess the functional consequences of FYN and c-ABL inhibition concerning F-actin disassembly, we treated the WT and KO AGCCs with FYN inhibitor PP2 (Fig. 6*A*) and c-ABL inhibitor imatinib (Fig. 6*B*). They effectively reduced F-actin disassembly in WT but not KO AGCCs. This finding suggested that reduced FYN and c-ABL activities occurred downstream

Figure 2. The effect of sex hormones on cortical F-actin disassembly in AGCCs from Ephb6 KO and WT mice. AGCCs isolated from KO and WT mice were cultured for 24 h and then stimulated with nicotine (50 μM) for 0, 20, 40, or 60 s. The cells were stained with rhodamine-conjugated phalloidin for F-actin and then analyzed according to confocal microscopy. At least 60 AGCCs per adrenal gland per mouse were examined for F-actin disassembly, which was defined as the gaps in the cortical F-actin ring that exceeded more than 5% of the circumference. Three independent experiments, each using one male KO and WT mouse, were performed, and the data of the three experiments were analyzed by a paired two-way test, mean ± S.E. were presented. Significant *p* values (Student's *t* test after arcsine transformation) between the WT and KO AGCCs at a given time point are shown. *A,* representative micrographs of cortical F-actin rings in WT AGCCs before and after 40-s nicotine stimulation. The *arrowheads* indicate gaps in the cortical F-actin ring. *Scale bar* = 2 μm. *B,* male KO AGCCs presented reduced cortical F-actin disassembly, and castration abrogated this phenotype. *C,* castration did not affect cortical F-actin disassembly in male WT AGCCs. *D,* AGCCs of female KO and WT mice were similar in cortical F-actin disassembly. *E* and *F,* testosterone rapidly lowered cortical F-actin disassembly in female KO (*E*) but not female WT (*F*) AGCCs. AGCCs were treated with cell membrane-impermeable BSA-conjugated testosterone (1.1 μg/ml) or vehicle for 15 min at 37 °C before nicotine stimulation. *G* and *H,* estrogen did not affect cortical F-actin disassembly in AGCCs from male WT (*G*) or KO (*H*) mice. AGCCs were treated with 17β-estradiol (100 pg/ml) or vehicle for 15 min at 37 °C before nicotine stimulation. *I,* short-term testosterone treatment lowered NE released from female KO but not from WT AGCCs. Cells obtained for female KO and WT AGCCs (10,000 cells per well) were cultured for 16 h and then treated with BSA-conjugated testosterone (1.1 μg/ml) or BSA in Hank's buffer at 37 °C for 15 min, and stimulated with 5 mM ACh for 1 min at room temperature. NE in the supernatants was measured and normalized to baseline NE secretion by female WT AGCCs without testosterone pretreatment or ACh stimulation. Normalized fold-changes (mean ± S.D.) of NE secretion of samples with different treatments are shown. Three independent experiments were conducted. Significant *p* values (2-way paired Student's *t* test) are indicated. Additional statistical analysis for the changes between different points in time is presented in Table S1.

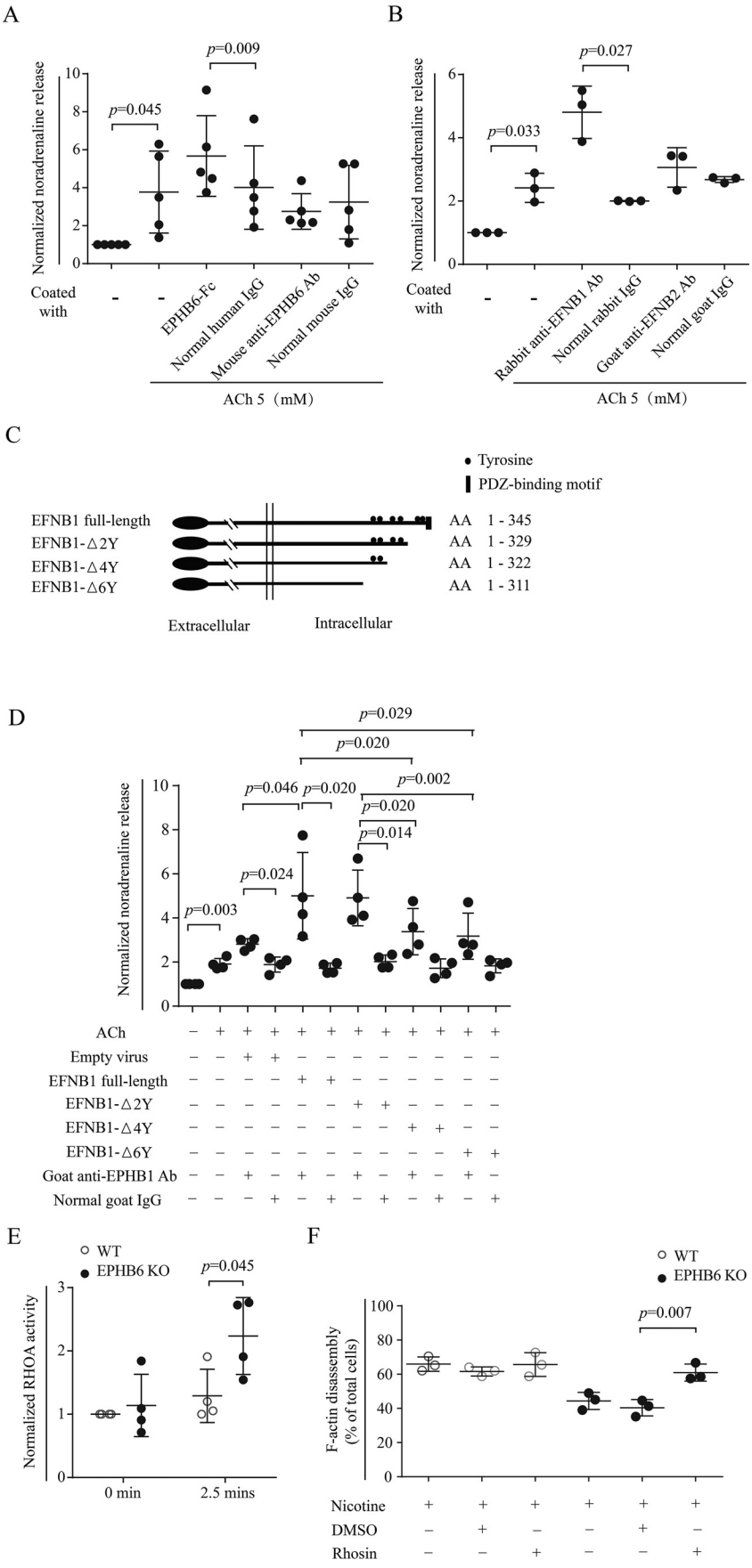
A
Normalized noradrenaline release
p=0.045
p=0.009
Coated with
-
-
EPHB6-Fc
Normal human IgG
Mouse anti-EPHB6 Ab
Normal mouse IgG
ACh 5 (mM)
B
Normalized noradrenaline release
p=0.033
p=0.027
Coated with
-
-
Rabbit anti-EFNB1 Ab
Normal rabbit IgG
Goat anti-EFNB2 Ab
Normal goat IgG
ACh 5 (mM)
C
Tyrosine
PDZ-binding motif
EFNB1 full-length AA 1 - 345
EFNB1-△2Y AA 1 - 329
EFNB1-△4Y AA 1 - 322
EFNB1-△6Y AA 1 - 311
Extracellular
Intracellular
D
Normalized noradrenaline release
p=0.003
p=0.024
p=0.046
p=0.020
p=0.029
p=0.020
p=0.002
p=0.020
p=0.014
ACh
Empty virus
EFNB1 full-length
EFNB1-△2Y
EFNB1-△4Y
EFNB1-△6Y
Goat anti-EPHB1 Ab
Normal goat IgG
E
WT
EPHB6 KO
p=0.045
Normalized RHOA activity
0 min
2.5 mins
F
WT
EPHB6 KO
p=0.007
F-actin disassembly (% of total cells)
Nicotine
DMSO
Rhosin

of EPHB6, and were relevant to the reduced F-actin disassembly seen in the make KO AGCCs.

Discussion

In this work, we demonstrated that EPHB6 reverse signaling via a 7-aa intracellular sequence of EFNB1 between aa 322 and 328 was critical for regulating CAT exocytosis in AGCCs. The signaling from EFNB1 traversing through RHOA as well as through the FYN/c-ABL/MICAL-1/F-actin pathways was necessary for EPHB6's effect on CAT secretion.

In our amperometric experiments, CAT vesicles released within 2 and 60 s after ACh stimulation were recorded. A reduced number of spikes during the first 2 s in KO AGCCs were found (Fig. 1*C*). Such reduction reflects reduced immediately-released CAT. This could be caused by the Ca^{2+} influx decrease in these cells, as we reported previously (19), or caused by a smaller pool of immediately-releasable vesicles (IRVs), or both, in the KO AGCCs. Additional experiments will be needed to assess the pool size of IRVs.

Analysis of individual spike parameters is commonly used to quantify the dynamics and size of single vesicular fusion events. We found here that the spike charge Q, reflecting the amount of CAT released per vesicle, was lower in male KO AGCCs, suggesting less catecholamine content in the vesicles in action. This observation is in agreement with our previous report that the male KO AGCCs are compromised in their CAT biogenesis (24).

The maximal amplitude (I_{max}) of the spike is proportional to the rate of catecholamine release and is thus a function of the amount of catecholamine released and the discharge kinetics. $T_{½}$ and T_{peak} reflect the discharge kinetics. In the male KO AGCCs, the I_{max} but not $T_{½}$ or T_{peak} was significantly reduced, indicating that the discharge kinetics in the KO AGCCs was normal, and thus the reduced I_{max} is likely the consequence of a smaller amount of catecholamine released.

The pre-spike feet reflect the fusion pore formation between vesicular and cell membranes, and the small amount of CAT released during this process (36). PSFs per cell, PSF amplitude, and the percentage of PSF present in all spikes were all reduced in the male KO AGCCs, suggesting that EPHB6 was involved in the processes reflected by these parameters. However, the underlying mechanisms and significance of these PSF parameters concerning CAT exocytosis remained to be elucidated.

The cortical F-actin network in resting AGCCs forms a continuous net but is disassembled within seconds after ACh-triggered activation. Such a morphological change does not only allow CAT-containing vesicles in the reserve pool to pass the disrupted F-actin net to replenish the IRV pool but also plays an active role in the fusion of the IRVs with the cell membrane (37). EPHB6 deletion compromised such F-actin disassembly, and this likely also contributes to the decreased CAT exocytosis observed in KO AGCCs. If the role of meshed F-actin in preventing the vesicles in the reserve pool to move to IRV pool outweights its role in the fusion of vesicles to the cell membrane, then the role of EPHB6 is probably more critical in the sustained CAT release by AGCCs.

Our results also showed that the effect of EPHB6 KO in preventing F-actin disassembly depended on the presence of testosterone. This finding was corroborated by the decreased CAT release by female KO AGCCs in the presence of testosterone (Fig. 2*I*), and our previous in *vivo* results showing that male but not female KO mice presented decreased 24-h urine CAT levels (12).

EPHB6 can trigger signals into cells in two ways. The first is forward signaling from its ligand EFNs in neighboring cells to EPHB6 on the target cells, occurring through an intracellular sequence of EPHB6. Second is reverse signaling from EPHB6 on the neighboring cells to the EFNs on the target cells, occurring through the intracellular sequence of EFNBs. Through a series of solid-phase stimulations mimicking the cell-surface EPHB6 and EFNs, we determined that reverse signaling through EFNB1 but not forward signaling through EPHB6 was essential for EPHB6's effect on F-actin disassembly. Among the two critical features of the intracellular domain of EFNB1 (*i.e.* C-terminal PDZ-binding motif and 5 tyrosine residues potentially associating with SH domain-containing signaling molecules), our results showed that a 7-aa sequence between residues 322 and 328, which contains Tyr-323 and Tyr-328, was critical for CAT release. This region was previously shown to be essential to mediate T cell chemotaxis toward chemokine CXCL12 (38). For different cell types and in responses to various stimuli, different regions of the EFNB1 intracellular domain are implicated, leading to different biological outcomes. For example, in T cells, the 11-aa segment between residues 311 and 321 harboring Tyr-312 and Tyr-316 is indispensable for T cell chemotaxis to chemokine CCL21 (39); the 16-aa sequence contain-

Figure 3. EPHB6 to EFNB1 reverse signaling modulated NE secretion by AGCCs. tsAM5NE chromaffin cells were cultured in wells coated with anti-EPHB6 Ab, recombinant EPHB6-Fc, anti-EFNB1 Ab, anti-EFNB2 Ab, or their isotype control IgGs for 24 h, as indicated. The culture medium was replaced with Hank's buffer, and after 15 min, cells were stimulated with 5 mM ACh. One min later, supernatants were harvested for NE measurements. The baseline NE secretion by tsAM5NE cells cultured in uncoated wells without ACh stimulation was considered as 1-fold. The normalized fold-changes (mean ± S.D.) of the NE secretion of cells with different treatments are shown. Three to five independent experiments were conducted. Significant *p* values (2-way paired Student's *t* test) are indicated. *A,* the ACh-stimulated NE release by tsAM5NE cells was promoted by solid-phase EPHB6-Fc but not by anti-EPHB6 Ab. Data from 5 independent experiments were normalized and presented. *B,* solid-phase anti-EFNB1 Ab but not anti-EFNB2 Ab augmented ACh-stimulated NE release. The results from 3 independent experiments were normalized and presented. *C,* the structures of EFNB1 protein and its deletion mutants. *D,* identification of the critical intracellular sequence of EFNB1 in mediating reverse signaling. tsAM5NE cells were infected with lentiviruses encoding full-length and deletion mutants of *EFNB1,* as indicated. The infected cells were seeded in wells coated with anti-EFNB1 Ab or normal goat IgG for 24 h and then stimulated with ACh for 1 min. The ACh-stimulated NE release was measured. Data from 4 independent experiments were normalized and presented. *E,* the activity of RHOA after nicotine stimulation was elevated in adrenal medullae from male KO mice. Adrenal medullae were stimulated with nicotine (20 μM) for 0 and 2.5 min. The activated RHOA level in the adrenal medullae was measured by G-LISA. The RHOA activity of WT medulla at 0 min was considered as one-fold for normalization. The results of four independent experiments were normalized, and the fold-changes (mean ± S.D.) of different samples are presented. *F,* RHOA inhibitor reverted the low cortical F-actin disassembly in male KO AGCCs to a normal level. AGCCs isolated from male KO or WT mice were cultured for 1 day and then treated with Rhosin (30 μM) or DMSO in Opti-MEM™ Reduced Serum Media for 4 h at 37 °C. Cells were stimulated 40 s with nicotine (50 μM), and their cortical F-actin disassembly was assessed by confocal microscopy. The percentages (mean ± S.D.) of cells with F-actin disassembly from three independent experiments are presented. Significant *p* value (two-way paired Student's *t* test after arcsine transformation) is indicated.

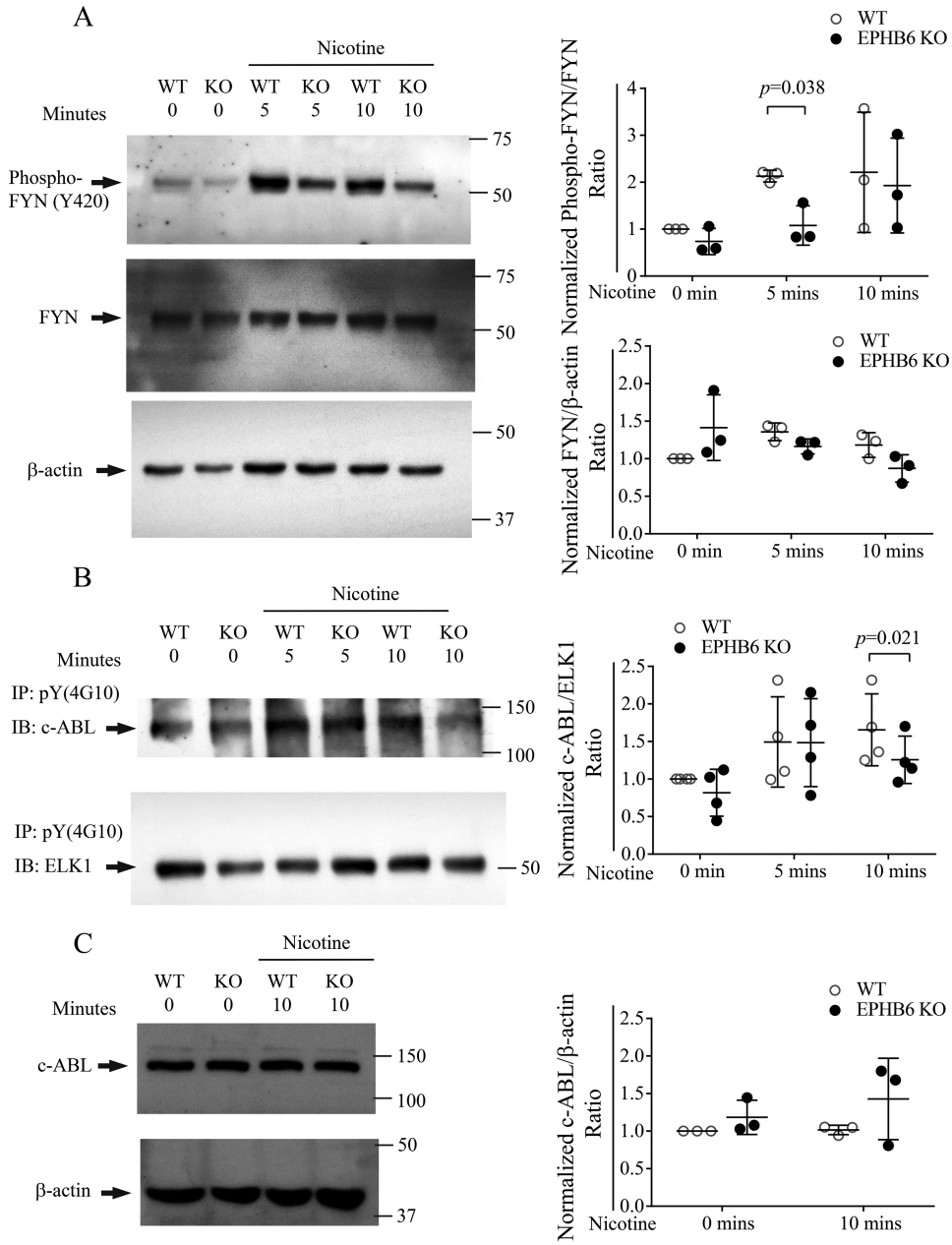

Figure 4. Decreased FYN and c-ABL phosphorylation in male KO adrenal medullae upon nicotine stimulation. Adrenal medullae from male WT and KO mice were stimulated with nicotine (20 μM) for 0 or 10 min at 37 °C. The phosphorylated FYN, total FYN phosphorylated c-ABL, total ABL, and β-actin levels of the medullae lysates were determined by immunoblotting. *A,* decreased FYN phosphorylation in medullae obtained from EPHB6 mice. Representative immunoblots of phosphorylated FYN (Y420) (*upper panel*), total FYN (*middle panel*), and β-actin (*bottom panel*) were shown. The densitometry signal ratios of phosphor-FYN *versus* FYN, and the ratio of total FYN *versus* β-actin of WT medullae at 0 min was used to normalize the data from 3 independent experiments. The normalized fold-changes (mean ± S.D.) were presented. The significant *p* values are indicated (2-way paired Student's *t* test). *B* and *C,* decreased c-ABL phosphorylation in the KO medullae. Lysate proteins from WT and KO medullae after 0- or 10-min nicotine stimulation were immunoprecipitated with anti-phosphoprotein Ab. The precipitated proteins were immunoblotted with anti-c-ABL or anti-ELK1 Ab. Representative immunoblots on the *left* show c-ABL and ELK phosphorylation (*B*) and total c-ABL and β-actin (*C*). The densitometry signal ratios of phospho-c-ABL *versus* phospho-ELK, and total c-ABL *versus* β-actin of WT medullae at 0 min were used to normalize the data from four independent experiments. The normalized fold-changes (mean ± S.D.) were presented on the *right*. The significant *p* values are indicated (2-way paired Student's *t* test).

ing Tyr-342 and Tyr-343 negatively regulates T cell chemotaxis to CXCL12; the 16-aa stretch from residues 331 to 345 is essential for RHOA activation and metalloproteinase secretion in gastric cancer cells (40). However, these regions did not have a perceptible effect on F-actin disassembly in AGCCs, based on our deletion study.

We tried to decipher the signaling pathways from the EFNB1 intracellular sequence to CAT exocytosis. Possible pathways elucidated in this study or described in the literature from EPHB6/EFNB1 to F-actin disassembly and concerning both CAT exocytosis are illustrated in Fig. 7. It seems that EFNB1 has a constitutively suppressive effect on RHOA activation in AGCCs. In its absence in KO AGCCs, such a suppressive effect was released, and hence the level of GTP-bound active RHOA was elevated. Active RHOA favors the maintenance of the cortical F-actin network in AGCCs (41–43) and inhibits AGCC

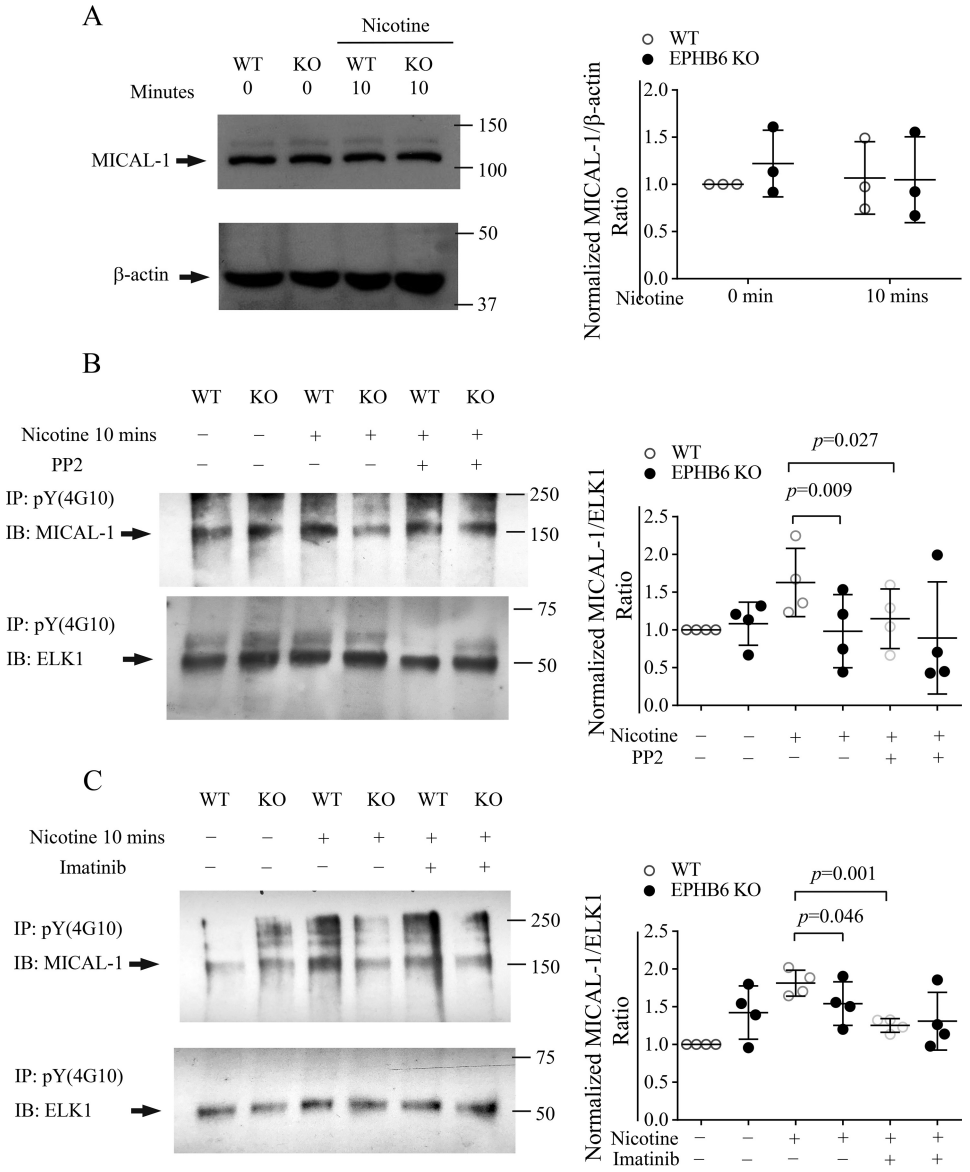

Figure 5. Reduced MICAL-1 phosphorylation in male KO adrenal medullae upon nicotine stimulation. Adrenal medullae from male WT and KO mice were cultured in the absence or presence of FYN inhibitor PP2 (10 μM) or c-ABL inhibitor Imatinib (20 μM), as indicated, at 37 °C for 2 h, and then stimulated with nicotine (20 μM) for 10 min. Their lysates were immunoprecipitated with anti-phosphoprotein Ab 4G10 and blotted with anti-MICAL-1 and ELK1 Abs. The densitometry signal ratios of total MICAL-1 *versus* β-actin and phospho-MICAL-1 *versus* phospho-ELK in WT male medullae without nicotine stimulation were used to normalize the data from four independent experiments. Representative immunoblots are shown on the *left*, and normalized fold-changes (mean ± S.D.) according to densitometry are shown on the *right*. The significant *p* values are indicated (2-way paired Student's *t* test). *A,* unchanged total MICAL-1 levels in male KO medullae. *B,* compromised MICAL-1 phosphorylation in KO medullae after nicotine stimulation, or in WT medullae treated with FYN inhibitor. *C,* decreased MICAL-1 phosphorylation in WT medullae treated with c-ABL inhibitor. The same membranes were sequentially blotted with anti-c-ABL (Fig. 4*C*), MICAL-1 and β-actin Abs, with a stripping process between these different immunoblottings. The same β-actin immunoblotting was used as loading controls for both Fig. 4*C* and *panel A*.

CAT secretion (31). Currently, the intermediate molecule linking the EFNB1 peptide sequence aa 323–328 to RHOA remains to be identified. This molecule might be a negative regulator of RHOA activity, such as GTPase-activating protein or a guanine nucleotide dissociating inhibitor (44). Alternatively, it might be an adaptor protein binding to RHOA regulators (40). Several pathways can lead to RHOA's activity to actin polymerization (45). We investigated one of them and found that the RHOA/ROCK/LIMK/COFILIN/F-actin pathway was not implicated (data not shown). We cannot exclude the possibility that the effect of EPHB6/EFNB1 reverse signaling on regulating RHOA activity is via the initially reduced Ca^{2+} influx (19). However, this possibility is incompatible with some literature and our findings. For example, the RHOA/ROCK/Ezrin pathway, which promotes F-actin stabilization, is positively regulated by Ca^{2+} influx and CaMKII (46, 47), as illustrated in Fig. 7. This implies that the reduced Ca^{2+} influx caused by EPHB6 KO would reduce RHOA activity, and consequently decreased F-actin stabilization, which favors CAT secretion but not reduced CAT secretion. Additional investigation is needed to firmly establish if there is Ca^{2+}-independent regulation of RHOA activity by the EPHB6/EFNB1 reverse signaling.

The other pathway from EPHB6/EFNB1 to F-actin involves FYN/c-ABL/MICAL/F-actin. Using FYN inhibitor PP2 and

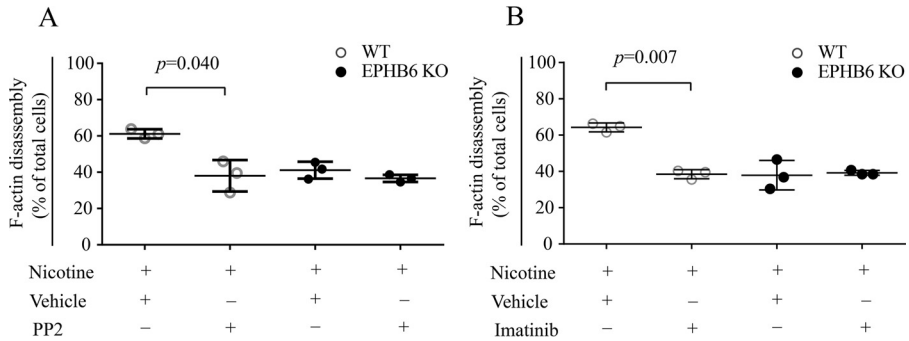

Figure 6. FYN and c-ABL inhibitor repressed cortical F-actin disassembly in male WT but not KO AGCCs. AGCCs isolated from male KO or WT mice were cultured for 24 h, and then cultured in the presence of PP2 (10 μM) (*A*) for 1 h or imatinib (20 μM) (*B*) for 2 h at 37 °C. The cells were stimulated with nicotine (50 μM) for 40 s, and their cortical F-actin disassembly was determined according to confocal microscopy. The percentages (mean ± S.D.) of cells with F-actin disassembly from three independent experiments are presented. The significant *p* values are indicated (2-way paired Student's *t* test).

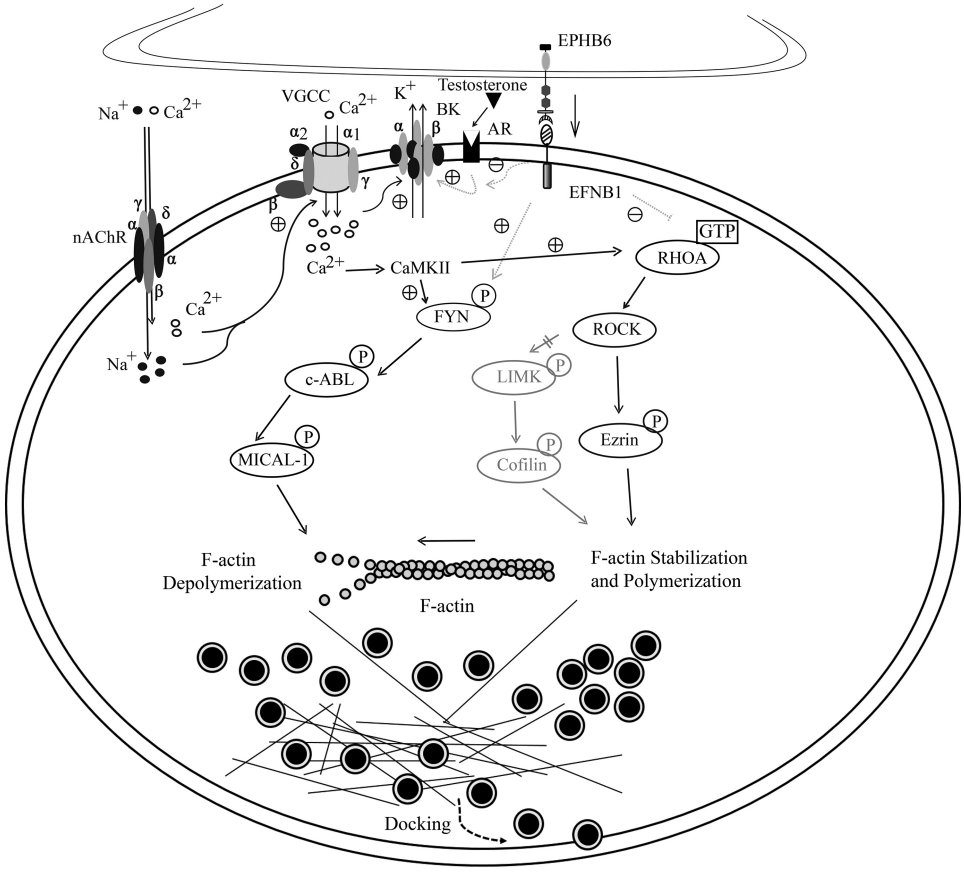

Figure 7. A diagram depicting signaling pathways from EPHB6 to CAT exocytosis in AGCCs. *Solid lines* represent pathways verified in this study or already established in the literature, whereas *faint dotted lines* depict speculated pathways. *Circles with black fillings* are CAT-containing vesicles. ACh activation of Ach receptor/gated ion channels triggers Na^+ and Ca^{2+} influx (74), subsequently amplified by voltage-gated calcium channels (*VGCC*). The depolarization and the increased Ca^{2+} concentration causes the opening of the BK, which repolarizes the cells and shuts down VGCC (75, 76). The nongenomic effect of testosterone positively regulates BK opening, whereas EPHB6 to EFNB1 reverse signaling negatively impacts on such an effect of testosterone (24, 77). Increased Ca^{2+} levels activate CaMKII (78), leading to activation of many downstream signaling events that enhance both CAT biogenesis (79) and exocytosis (this study). The FYN/c-ABL/MICAL-1 pathway that promotes F-actin depolymerization is downstream of and positively regulated by CaMKII (33–35, 80). The RHOA/ROCK/Ezrin pathway, which promotes F-actin stabilization, is also positively regulated by CaMKII (46, 47). Although the two pathways have opposite effects on F-actin disassembly after the Ca^{2+} influx, under normal circumstances, the balance is in favor of F-actin disassembly. The EPHB6 to EFNB1 reverse signaling by itself has no effect on CAT exocytosis. The effect of the defective reverse signaling on all the downstream events could be due to the initial compromised Ca^{2+} influx. It is also possible that such reverse signaling might modify signaling events directly. The reverse signaling might have a default direct positive effect on the FYN/c-ABL/MICAL-1/F-actin pathway. It might also have a direct default negative effect on RHOA activation, which promotes F-actin stabilization typically. ROCK/Ezrin (49) and ROCK/LIMK/Cofilin (50) pathways are known to be downstream of RHOA, although the latter is not activated in ACh-stimulated AGCCs (data not shown). F-actin depolymerization is not only essential in moving the slow-release CAT-containing vesicles to the docking position (51) but is also critical for optimal vesicular fusion and sewage of CAT content from the vesicles in the IRV pool during rapid exocytosis. In the absence of EPHB6/EFNB1 reverse signaling, as is the case in EPHB6 KO, the signaling strength of the FYN/c-ABL/MICAL pathway is compromised, whereas the signaling strength of RHOA/ROCK/Ezrin is relatively increased. These changes eventually lead to reduced F-actin disassembly and CAT exocytosis in the male KO AGCCs.

c-ABL inhibitor Imatinib, we showed that these inhibitors affected F-actin disassembly in WT but not in KO AGCCs, indicating that this pathway leading to F-actin is relevant to the EPHB6/EFNB1 reverse signaling and that it is not functional when EPHB6 is absent. FYN is likely immediately downstream of EFNB1, as the SRC family kinases are recruited to the lipid domain where EFNB1 is localized after the reverse signaling is triggered, and FYN is activated (45), although direct evidence of EFNB1 and FYN co-localization or interaction is still lacking. MICAL-1 is likely to be at the other end of this pathway, and its redox enzymatic activity may specifically destabilize F-actin (48). Again, it is possible that the observed effects of EPHB6/EFNB1 reverse signaling on the FYN/c-ABL/MICAL/F-actin pathway are due to its initial impact on the Ca^{2+} influx (19). The end results remain the same. In the absence of EPHB6 reverse signaling via EFNB1, MICAL-1 activity was reduced, leading to an increase in F-actin stability.

Although the above-mentioned two pathways have opposite effects on F-actin disassembly after the Ca^{2+} influx, under normal circumstances, the balance is in favor of F-actin disassembly. The EPHB6 to EFNB1 reverse signaling by itself has no effect on CAT exocytosis. The effect of the defective reverse signaling on all the downstream events could be due to the initial compromised Ca^{2+} influx, as mentioned above. It is also possible that such reverse signaling might modify signaling events directly in addition to its effect on Ca^{2+} influx. The reverse signaling might have a default direct positive effect on the FYN/c-ABL/MICAL-1/F-actin pathway. On the other hand, it might have a direct default negative effect on RHOA activation, which promotes F-actin stabilization typically. ROCK/Ezrin (49) and ROCK/LIMK/Cofilin (50) pathways are known to be downstream of RHOA, although the latter is not activated in ACh-stimulated AGCCs (data not shown). F-actin depolymerization is not only essential in moving the slow-release CAT-containing vesicles to the docking position (51) but is also critical for optimal vesicular fusion and sewage of CAT content from the vesicles in the IRV pool during rapid exocytosis. In the absence of EPHB6/EFNB1 reverse signaling, as is the case in EPHB6 KO, the signaling strength of the FYN/c-ABL/MICAL pathway is compromised, whereas the signaling strength of RHOA/ROCK/Ezrin is relatively increased. These changes eventually lead to reduced F-actin disassembly and CAT exocytosis in the male KO AGCCs.

We previously demonstrated that the male but not female EPHB6 KO AGCCs presented a lower Ca^{2+} influx after ACh stimulation (19). The difference in the Ca^{2+} influx between male and female KO AGCCs was due to the absence of testosterone but not the presence of estrogen in females (19). The ACh-triggered Ca^{2+} influx is the first and most important event leading to the activation of many downstream events. It is possible that some abnormal manifestations of these events in the KO cells are the consequence of the initially reduced Ca^{2+} influx. However, it is also possible that EPHB6/EFNB1 has Ca^{2+}-independent regulation of FYN and RHOA activation, as illustrated in Fig. 7 by faint dotted lines between EFNB1 and FYN, and between EFNB1 and RHOA. We could induce a maximal Ca^{2+} influx in AGCCs by ionomycin. If under such a circumstance, the activation of the FYN and/or RHOA pathways is still different in the WT and KO AGCCs, then we could conclude that indeed Ca^{2+} influx-independent regulation of FYN and RHOA activation by EPHB6/EFNB1 reverse signaling does exist. Such experiments will be performed shortly.

Although F-actin disassembly became obvious only 20 s after nicotine stimulation, it is conceivable that some more subtle actin disassembly, not measurable with our experimental approach, had already occurred in the first several seconds after stimulation. This rapid kinetics is compatible with that of acute CAT secretion, which happens at a similar time scale and is consistent with the more recently described positive role of F-actin disassembly in vesicle fusion (52). Of course, the disassembly is also essential in mobilizing the vesicles from the reserve pool for chronic CAT secretion (51), which is probably more relevant to hypertension caused by chronic stress and chronic sterile inflammation (53–55). In our study, the FYN/c-ABL/MICAL-1 pathway activation was demonstrated to occur 5–10 min after nicotine stimulation. Such slow kinetics is probably pertinent to the chronic CAT secretion, which requires F-actin disassembly and slow-releasing vesicle mobilization at such a time scale. However, FYN and c-ABL inhibitors effectively suppressed F-actin disassembly in 20 s after nicotine stimulation (Fig. 6, *A* and *B*), proving that this pathway is also essential in acute CAT secretion. Likely, immunoblotting of FYN, c-ABl, and MICAL-1 phosphorylation is not sensitive to detect earlier activation of this pathway within seconds of nicotine stimulation.

The major sources of blood EPI and NE are AGCCs and the nervous system, respectively, whereas the blood dopamine level is very low. Blood pressure increase during acute stress is associated with EPI released from AGCCs. There are different opinions regarding whether the blood EPI level is associated with blood pressure under nonstress conditions. Early publications showed that ambient EPI levels are associated with blood pressure in humans and animals (56–61). In recent years, chronic stress (53, 54) and systemic sterile low-level chronic inflammation are found to be significant contributing factors of primary hypertension (55). These conditions are associated with elevated blood NE levels derived from the nervous system, but increased EPI levels from AGCCs are also often observed (62–67). In a mouse model, augmented catecholamine release from AGCCs caused by TRPM4 deletion has been shown to cause hypertension (68). These data suggest that the excessive CAT release from the adrenal glands is a contributing factor to hypertension. In the case of EPHB6 mutation, hypogonadism causes an increase of CAT secretion from a depressed to a normal level.

Based on our previous and current findings along with existing literature, it is postulated that EPHB6 acts in concert with testosterone to regulate blood pressure. EPHB6/EFNB1 reverse signaling has a positive constitutive effect on CAT biosynthesis (24) and exocytosis, but such effects depend on the presence of testosterone. In the absence of the said reverse signaling due to EPHB6 deletion in individuals with a normal level of testosterone, the ambient CAT biosynthesis and secretion are reduced. Such reduction tends to lower blood pressure, but EPHB6 KO loss-of-function mutations also cause increased resistant artery constriction due to its other function on vascular smooth mus-

cle cells (12), inclined toward an increase in blood pressure. These two opposite effects on blood pressure cancel out each other, and the final outcome is that in EPHB6 KO/mutations males with sufficient testosterone, their blood pressure remains normal. However, if patients with EPHB6 loss-of-function mutations or defective EPHB6-EFNB1 reverse signaling become hypogonadic (castration in the case of mice), their CAT biosynthesis and exocytosis return to the normal level. At the same time, due to the vasoconstrictive effect of EPHB6 KO/mutation, the resistance of blood flow is increased, and hence their blood pressure is augmented. For these patients, testosterone could be a personalized medication for hypertension.

Experimental procedures

Ephb6 gene KO mice

Ephb6 KO mice were generated in our laboratory, as described previously (69). They were backcrossed to the C57BL/6J genetic background for more than 15 generations. Age- and gender-matched WT littermates served as controls. Some male mice underwent castration, and they were used 3 weeks after the surgery.

Primary AGCC culture for amperometry recording

Mouse AGCCs were isolated, as described earlier (70), with modifications. Adrenal glands were obtained from 8- to 12-week old mice. Medullae were separated from fat and cortex in cold Locke's solution then digested with 5 units of papain activated in Dulbecco's modified Eagle's medium (DMEM) containing 0.2 mg/ml of L-cysteine, 1 mM $CaCl_2$, 0.5 mM EDTA, 0.0067 mM β-mercaptoethanol (200 ml for 2 medullae) at 37 °C for 20 min. Papain digestion was stopped with 100 μl of an inactivating solution DMEM, 10% deactivated fetal calf serum (FCS), 1.25 mg/ml of albumin, 1.25 mg/ml of trypsin-inhibitor) and incubated for 5 min at 37 °C. The digested medullae were triturated by pipetting in 300 μl of complete culture medium (DMEM, 1/500 primocin, 1/100 ITSX). Cells were seeded in collagen-coated glass coverslips, complete culture medium was added 1 h later. Cells were maintained at 37 °C, 5% CO_2 for 24–48 h before amperometry recording.

Amperometry

Chromaffin cells from *Ephb6* WT and KO mice were washed with Locke's solution and processed for CAT release measurements by amperometry, which was conducted at room temperature. A carbon fiber electrode of 5-μm diameter (ALA Scientific, New York) was held at a potential of 650 mV compared with the reference electrode (Ag/AgCl) and was approached closely to the cells. The secretion of CAT was induced by 10-s pressure ejection of 100 μM nicotine in Locke's solution from a micropipette positioned at 10 μm from the cell and recorded over 60 s. Amperometric recordings were performed with an AMU130 amplifier (Radiometer Analytical, Loveland, CO), sampled at 5 kHz, and digitally low-pass filtered at 1 kHz. The analysis of amperometric recordings was carried out as previously described (71) with Macro software (obtained from the laboratory of Dr. R. Borges) written for Igor Software (Wavemetrics, Portland, OR), allowing automatic spike detection and extraction of spike parameters. The number of amperometric spikes with an amplitude >5 pA within 60 s after ACh stimulation was registered. The spike parameter analysis was restricted to these spikes with amplitudes of >5 pA. The quantal size of individual spikes was measured by calculating the spike area above the baseline (72). For PSF signals, the analysis was restricted to spikes with foot amplitudes of >2 pA. Cells responding by fewer than 5 spikes during the 60 s were excluded from the analysis, and so were spikes that partially overlapped with another spike. The number of spikes and PSFs were averaged per cell for 2 or 60 s after ACh stimulation. All the other amperometric parameters were calculated according to all the events in all the cells tested during the 60-s recording period.

Primary AGCC culture for biochemical and confocal microscopic analyses

Mouse AGCCs were isolated, as described by Kolski-Andreaco *et al.* (73), with modifications. The adrenal glands were obtained from 8- to 10-week-old mice. The fat and cortex were removed from the medullae, which were then digested with activated papain (P4762, Sigma-Aldrich, Oakville, Ontario, Canada) in Hank's buffer (2 medullae/100 μl of Hank's buffer containing 4 units of activated papain) at 37 °C for 25 min. The digested medullae were washed twice with Hank's buffer and triturated by pipetting in 300 μl of Hank's buffer until they became feather-like. Cells were pelleted at 3,700 × *g* for 3 min and re-suspended in DMEM containing 15% FCS for culture.

Confocal microscopy of F-actin

AGCCs were cultured in 6-well-plates with coverglass placed at the bottom of the wells. After 1 day, the cells were washed once with pre-warmed PBS and stimulated with nicotine (50 μm) for 0, 20, 40, and 60 s. The cells were then washed once with PBS and fixed with paraformaldehyde (4%) in PBS for 10 min at room temperature. They were permeabilized with 0.1% Triton X-100 in PBS for 3 min. The cells were labeled with rhodamine-conjugated phalloidin (1 unit/ml; R415, ThermoFisher Scientific, Burlington, Ontario, Canada) at room temperature for 20 min and imbedded with ProLong® Gold antifade reagent (Invitrogen, Burlington, Ontario, Canada). All labeled cells were viewed under a confocal microscope (Leica TCS SP5 MP, Allendale, NJ). The integrity of the cortical polymerized F-actin ring of each cell was assessed. At least 60 randomly selected AGCCs per treatment per mouse were examined. If gaps in the cortical F-actin rings were more than 5% the length of the circumference, the rings were considered disassembled.

Chromaffin cell line culture

AGCC line tsAM5NE cells were cultured in collagen IV-coated 24-well flat-bottom wells (Corning, New York, number 354430) in DMEM containing 15% FCS and G5 supplement (ThermoFisher Scientific, Burlington, Ontario, Canada; 17503012) in an environment of 5% CO_2 at 33 °C. In some experiments, these cells were cultured in wells coated with goat anti-EPHB6 Ab (AF611, R&D Systems, Oakville, Ontario, Canada), normal goat IgG (sc-2028, Santa Cruz Biotechnology, Mississauga, Ontario, Canada), recombinant EPHB6-Fc

(E9777, Sigma-Aldrich), or normal human IgG (0150-01, Southern Biotech, Birmingham, AL) (2 μg/ml during overnight coating at 4 °C) for 24 h. Nicotine (40 μM) was used to stimulate these cells.

G-LISA assays for activated RHOA

Adrenal medullae were isolated from *Ephb6* KO and WT male mice, and cultured in Opti-MEM™ Reduced Serum Media at 37 °C for 2 h. Nicotine (20 μM) was used to stimulate the adrenal medulla for 2.5 min, which was determined as the peak activation time according to pilot studies. Proteins were extracted from the tissues on ice for 5 min in G-LISA's cell lysis buffers containing protease inhibitor cocktails (Cytoskeleton, Inc., Denver, CO; BK128). The cleared supernatants were snap-frozen in liquid nitrogen and stored at −80 °C until the assay. Activated RHOA G-protein within samples (25 μg/sample) were determined by the G-LISA assay (Cytoskeleton, Inc.) according to the manufacturer's instructions. Samples were assayed in duplicate.

NE measurements

tsAM5NE AGCCs were cultured for 24 h. The cells were washed once by pre-warmed Hank's buffer and placed in Hank's buffer at 37 °C for 15 min. Then these cells were stimulated with 5 mM ACh chloride (A2661, Sigma-Aldrich) in Hank's buffer for 1 min. NE levels in the supernatants were measured with the NE Research ELISA kit (BA E-5200, Rocky Mountain Diagnostics, Colorado Springs, CO) according to the manufacturer's instructions. Each sample was tested in duplicate. In some experiments, 10,000 AGCCs from WT or *Ephb6* KO female mice were cultured in collagen IV-coated 24-well-plates in DMEM with 15% FCS for 16 h at 37 °C. These cells were treated with BSA-conjugated testosterone (1.1 μg/ml, testosterone-3-(O-carboxymethyl)-oxime-BSA; Aviva Systems Biology, San Diego, CA) or BSA in Hank's buffer at 37 °C for 15 min after washing once by pre-warmed Hank's buffer. The cells were then stimulated with ACh (5 mM) for 1 min. The supernatants were harvested and tested for NE levels by ELISA.

Lentivirus preparation and infection

Polymerase chain reaction (PCR)-based deletion mutations of *Efnb1* intracellular tails were generated and cloned into the pLentiviral CMV/TO PGK GFP Destination vector (Addgene) as previously described (38). The expression plasmid, control plasmid, and packaging constructs plp1, plp2, and plpSV were transfected into HEK 293T cells. The viruses were harvested by collecting the supernatant 72 h later and concentrated by ultra-centrifugation. tsAM5NE cells (1.2×10^5 cells/well in 24-well-plates) were transfected with lentiviruses in the presence of 10 μg/ml of Polybrene (sc-134220, Santa Cruz Biotechnology) immediately after passage. After 72 h, the transfected cells were re-plated (1.2×10^5 cells/well) in 24-well-plates coated with collagen IV plus goat anti-EFNB1 Ab (AF473, R&D Systems), or normal goat IgG (sc-2028, Santa Cruz Biotechnology) for 24 h before the measurement of ACh-stimulated NE secretion.

Immunoprecipitation and immunoblotting

Adrenal gland medullae were collected from 8- to 10-week-old WT and *Ephb6* KO male mice, and rested in DMEM at 37 °C for 2 h. They were stimulated with nicotine (20 μm) for 5 or 10 min at 37 °C and then lysed by immunoprecipitation assay buffer (RIPA), which contained PhosSTOP and a protease inhibitor mixture (Roche Applied Science, Meylan Cedex, France). Sixty μg of lysate protein/sample was resolved on 7.5% SDS-PAGE and transferred to polyvinylidene difluoride membranes (Invitrogen). In some experiments, the lysates were precleared with protein G magnetic beads (1614023, Bio-Rad Laboratories), and then precipitated with anti-phosphotyrosine Ab 4G10 (05321, Sigma) plus protein G magnetic beads at 4 °C overnight with gentle rotation. The precipitated proteins were resolved in 7.5% SDS-PAGE and transferred to polyvinylidene difluoride membranes. The membranes were blotted with mouse anti-phospho-FYN (Y420) Ab (STJ110851, St. John's laboratory, London, UK), mouse anti-FYN-59 Ab (626502, Biolegend, San Diego, CA), rabbit anti-c-ABL Ab (2862, Cell Signaling Technology, Danvers, MA), rabbit anti-MICAL1 Ab (ab181145, Abcam), rabbit anti-ELK1 Ab (9182; Cell Signaling Technology), or rabbit anti-β-actin Ab (4967; Cell Signaling Technology). All the Abs were used at the manufacturers' recommended dilutions. Signals were visualized by SuperSignal West Pico Chemiluminescent Substrate (ThermoFisher Scientific).

Ethics statement

All the animal studies were approved by the Animal Protection Committee (Comité institutionnel d'intégration de la protection des animaux) of the CRCHUM or conducted according to European Council Directive 86/609/EEC.

Data availability

All the data supporting our conclusions are presented in this article.

Author contributions—W. S., B. Y., and N. V. formal analysis; W. S., B. Y., and N. V. validation; W. S., B. Y., M. R., D. C., and S. R. F. investigation; W. S., B. Y., M. R., Y. W., D. C., S. R. F., J. P., S. Q., N. V., H. L., and J. W. methodology; W. S., B. Y., N. V., H. L., and J. W. writing-original draft; M. R., Y. W., N. V., H. L., and J. W. funding acquisition; N. V., H. L., and J. W. supervision; N. V., H. L., and J. W. project administration; H. L. and J. W. conceptualization.

Funding and additional information—This work was supported by grants from the Fonds de recherche du Québec-Santé and the J.-Louis Lévesque Foundation (to J. W.), Canadian Institutes of Health Research Grant MOP272014 (to J. W.) Natural Sciences and Engineering Research Council of Canada Grant RGPIN-2017-04790 (to J. W.) and a Agence Nationale de la Recherche grant (to N. V.) and Fondation pour la Recherche Médicale grant DEI20151234424 (to N. V.), and National Natural Science Foundation of China Grant 81700363 (to Y. W.).

Conflict of interest—The authors declare that they have no conflicts of interest with the contents of this article.

Abbreviations—The abbreviations used are: EPH, erythropoietin-producing human hepatocellular receptors; EFN, ephrins; AGCC,

adrenal gland chromaffin cell; KO, knockout; CAT, catecholamine; ACh, acetylcholine; BK, big potassium channel; PSF, pre-spike feet; EPI, epinephrine; NE, norepinephrine; IRV, immediately-releasable vesicle; Ab, antibody; aa, amino acid(s); DMEM, Dulbecco's modified Eagle's medium; FCS, fetal calf serum; IP, immunoprecipitation; IB, immunoblot.

References

1. Eph Nomenclature Committee. (1997) Unified nomenclature for Eph family receptors and their ligands, the ephrins. *Cell* **90,** 403–404 CrossRef Medline
2. Pasquale, E. B. (2008) Eph-ephrin bidirectional signaling in physiology and disease. *Cell* **133,** 38–52 CrossRef Medline
3. Flanagan, J. G., and Vanderhaeghen, P. (1998) The ephrins and Eph receptors in neural development. *Annu. Rev. Neurosci.* **21,** 309–345 CrossRef Medline
4. Holmberg, J., Genander, M., Halford, M. M., Anneren, C., Sondell, M., Chumley, M. J., Silvany, R. E., Henkemeyer, M., and Frisén, J. (2006) EphB receptors coordinate migration and proliferation in the intestinal stem cell niche. *Cell* **125,** 1151–1163 CrossRef Medline
5. Zhao, C., Irie, N., Takada, Y., Shimoda, K., Miyamoto, T., Nishiwaki, T., Suda, T., and Matsuo, K. (2006) Bidirectional ephrinB2-EphB4 signaling controls bone homeostasis. *Cell Metab.* **4,** 111–121 CrossRef Medline
6. Brantley-Sieders, D. M., and Chen, J. (2004) Eph receptor tyrosine kinases in angiogenesis: from development to disease. *Angiogenesis* **7,** 17–28 CrossRef Medline
7. Wu, J., and Luo, H. (2005) Recent advances on T-cell regulation by receptor tyrosine kinases. *Curr. Opin. Hematol.* **12,** 292–297 CrossRef Medline
8. Konstantinova, I., Nikolova, G., Ohara-Imaizumi, M., Meda, P., Kucera, T., Zarbalis, K., Wurst, W., Nagamatsu, S., and Lammert, E. (2007) EphA-Ephrin-A-mediated beta cell communication regulates insulin secretion from pancreatic islets. *Cell* **129,** 359–370 CrossRef Medline
9. Hashimoto, T., Karasawa, T., Saito, A., Miyauchi, N., Han, G. D., Hayasaka, K., Shimizu, F., and Kawachi, H. (2007) Ephrin-B1 localizes at the slit diaphragm of the glomerular podocyte. *Kidney Int.* **72,** 954–964 CrossRef Medline
10. Salvucci, O., de la Luz Sierra, M., Martina, J. A., McCormick, P. J., and Tosato, G. (2006) EphB2 and EphB4 receptors forward signaling promotes SDF-1-induced endothelial cell chemotaxis and branching remodeling. *Blood* **108,** 2914–2922 CrossRef Medline
11. Dravis, C., Wu, T., Chumley, M. J., Yokoyama, N., Wei, S., Wu, D. K., Marcus, D. C., and Henkemeyer, M. (2007) EphB2 and ephrin-B2 regulate the ionic homeostasis of vestibular endolymph. *Hear. Res.* **223,** 93–104 CrossRef Medline
12. Luo, H., Wu, Z., Tremblay, J., Thorin, E., Peng, J., Lavoie, J. L., Hu, B., Stoyanova, E., Cloutier, G., Qi, S., Wu, T., Cameron, M., and Wu, J. (2012) Receptor tyrosine kinase Ephb6 regulates vascular smooth muscle contractility and modulates blood pressure in concert with sex hormones. *J. Biol. Chem.* **287,** 6819–6829 CrossRef Medline
13. Wu, Z., Luo, H., Thorin, E., Tremblay, J., Peng, J., Lavoie, J. L., Wang, Y., Qi, S., Wu, T., and Wu, J. (2012) Possible role of Efnb1 protein, a ligand of Eph receptor tyrosine kinases, in modulating blood pressure. *J. Biol. Chem.* **287,** 15557–15569 CrossRef
14. Wang, Y., Thorin, E., Luo, H., Tremblay, J., Lavoie, J. L., Wu, Z., Peng, J., Qi, S., and Wu, J. (2015) EPHB4 protein expression in vascular smooth muscle cells regulates their contractility, and EPHB4 deletion leads to hypotension in mice. *J. Biol. Chem.* **290,** 14235–14244 CrossRef
15. Wang, Y., Hamet, P., Thorin, E., Tremblay, J., Raelson, J., Wu, Z., Luo, H., Jin, W., Lavoie, J. L., Peng, J., *et al.* (2016) Reduced blood pressure after smooth muscle EFNB2 deletion and the potential association of EFNB2 mutation with human hypertension risk. *Eur. J. Hum. Genet.* **24,** 1817–1825 CrossRef Medline
16. Wang, Y., Wu, Z., Thorin, E., Tremblay, J., Lavoie, J. L., Luo, H., Peng, J., Qi, S., Wu, T., and Chen, F. (2016) Estrogen and testosterone in concert with EFNB3 regulate vascular smooth muscle cell contractility and blood pressure. *Am. J. Physiol. Heart Circ. Physiol.* **310,** H861–H872 CrossRef
17. Wang, Y., Wu, Z., Luo, H., Peng, J., Raelson, J., Ehret, G. B., Munroe, P. B., Stoyanova, E., Qin, Z., Cloutier, G., Bradley, W. E., Wu, T., Shen, J. Z., Hu, S., and Wu, J. (2016) The role of GRIP1 and ephrin B3 in blood pressure control and vascular smooth muscle cell contractility. *Sci. Rep.* **6,** 38976 CrossRef Medline
18. Tremblay, J., Wang, Y., Raelson, J., Marois-Blanchet, F. C., Wu, Z., Luo, H., Bradley, E., Chalmers, J., Woodward, M., Harrap, S., Hamet, P., and Wu, J. (2017) Evidence from single nucleotide polymorphism analyses of ADVANCE study demonstrates EFNB3 as a hypertension risk gene. *Sci. Rep.* **7,** 44114 CrossRef Medline
19. Wang, Y., Shi, W., Blanchette, A., Peng, J., Qi, S., Luo, H., Ledoux, J., and Wu, J. (2018) EPHB6 and testosterone in concert regulate epinephrine release by adrenal gland chromaffin cells. *Sci. Rep.* **8,** 842 CrossRef Medline
20. Wu, T., Zhang, B. Q., Raelson, J., Yao, Y. M., Wu, H. D., Xu, Z. X., Marois-Blanchet, F. C., Tahir, M. R., Wang, Y., Bradley, W. E., Luo, H., Wu, J., Sheng, J. Z., and Hu, S. J. (2018) Analysis of the association of EPHB6, EFNB1 and EFNB3 variants with hypertension risks in males with hypogonadism. *Sci. Rep.* **8,** 14497 Medline
21. Zhang, Z., Tremblay, J., Raelson, J., Sofer, T., Du, L., Fang, Q., Argos, M., Marois-Blanchet, F. C., Wang, Y., Yan, L., Chalmers, J., Woodward, M., Harrap, S., Hamet, P., Luo, H., and Wu, J. (2019) EPHA4 regulates vascular smooth muscle cell contractility and is a sex-specific hypertension risk gene in individuals with type 2 diabetes. *J. Hypertens.* **37,** 775–789 CrossRef Medline
22. Douglas, W. W., and Rubin, R. P. (1961) The role of calcium in the secretory response of the adrenal medulla to acetylcholine. *J. Physiol.* **159,** 40–57 CrossRef Medline
23. Haycock, J. W., Meligeni, J. A., Bennett, W. F., and Waymire, J. C. (1982) Phosphorylation and activation of tyrosine hydroxylase mediate the acetylcholine-induced increase in catecholamine biosynthesis in adrenal chromaffin cells. *J. Biol. Chem.* **257,** 12641–12648 Medline
24. Shi, W., Wang, Y., Peng, J., Qi, S., Vitale, N., Kaneda, N., Murata, T., Luo, H., and Wu, J. (2019) EPHB6 controls catecholamine biosynthesis by up-regulating tyrosine hydroxylase transcription in adrenal gland chromaffin cells. *J. Biol. Chem.* **294,** 6871–6887 CrossRef Medline
25. Kohno, S., Murata, T., Koide, N., Hikita, K., and Kaneda, N. (2011) Establishment and characterization of a noradrenergic adrenal chromaffin cell line, tsAM5NE, immortalized with the temperature-sensitive SV40 T-antigen. *Cell Biol. Int.* **35,** 325–334 CrossRef Medline
26. Tomlinson, A., Durbin, J., and Coupland, R. E. (1987) A quantitative analysis of rat adrenal chromaffin tissue: morphometric analysis at tissue and cellular level correlated with catecholamine content. *Neuroscience* **20,** 895–904 CrossRef Medline
27. Vollmer, R. R., Baruchin, A., Kolibal-Pegher, S. S., Corey, S. P., Stricker, E. M., and Kaplan, B. B. (1992) Selective activation of norepinephrine- and epinephrine-secreting chromaffin cells in rat adrenal medulla. *Am. J. Physiol.* **263,** R716–R721 Medline
28. Cho, H. J., Hwang, Y. S., Yoon, J., Lee, M., Lee, H. G., and Daar, I. O. (2018) EphrinB1 promotes cancer cell migration and invasion through the interaction with RhoGDI1. *Oncogene* **37,** 861–872 CrossRef Medline
29. O'Neill, A. K., Kindberg, A. A., Niethamer, T. K., Larson, A. R., Ho, H. H., Greenberg, M. E., and Bush, J. O. (2016) Unidirectional Eph/ephrin signaling creates a cortical actomyosin differential to drive cell segregation. *J. Cell Biol.* **215,** 217–229 CrossRef Medline
30. Tanaka, M., Kamo, T., Ota, S., and Sugimura, H. (2003) Association of Dishevelled with Eph tyrosine kinase receptor and ephrin mediates cell repulsion. *EMBO J.* **22,** 847–858 CrossRef Medline
31. Bader, M. F., Doussau, F., Chasserot-Golaz, S., Vitale, N., and Gasman, S. (2004) Coupling actin and membrane dynamics during calcium-regulated exocytosis: a role for Rho and ARF GTPases. *Biochim. Biophys. Acta* **1742,** 37–49 CrossRef Medline
32. Palmer, A., Zimmer, M., Erdmann, K. S., Eulenburg, V., Porthin, A., Heumann, R., Deutsch, U., and Klein, R. (2002) EphrinB phosphorylation and reverse signaling: regulation by Src kinases and PTP-BL phosphatase. *Mol. Cell* **9,** 725–737 CrossRef Medline
33. Plattner, R., Kadlec, L., DeMali, K. A., Kazlauskas, A., and Pendergast, A. M. (1999) c-Abl is activated by growth factors and Src family kinases

and has a role in the cellular response to PDGF. *Genes Dev.* **13,** 2400–2411 CrossRef Medline
34. Yoon, J., Kim, S. B., Ahmed, G., Shay, J. W., and Terman, J. R. (2017) Amplification of F-actin disassembly and cellular repulsion by growth factor signaling. *Dev. Cell* **42,** 117–129.e118 Medline
35. Hung, R. J., Pak, C. W., and Terman, J. R. (2011) Direct redox regulation of F-actin assembly and disassembly by Mical. *Science* **334,** 1710–1713 CrossRef Medline
36. Gong, L. W., de Toledo, G. A., and Lindau, M. (2007) Exocytotic catecholamine release is not associated with cation flux through channels in the vesicle membrane but Na^+ influx through the fusion pore. *Nat. Cell Biol.* **9,** 915–922 CrossRef Medline
37. Gutiérrez, L. M., and Villanueva, J. (2018) The role of F-actin in the transport and secretion of chromaffin granules: an historic perspective. *Pflugers Arch.* **470,** 181–186 CrossRef Medline
38. Hu, Y., Wang, X., Wu, Y., Jin, W., Cheng, B., Fang, X., Martel-Pelletier, J., Kapoor, M., Peng, J., and Qi, S. (2015) Role of EFNB1 and EFNB2 in mouse collagen-induced arthritis and human rheumatoid arthritis. *Arthritis Rheumatol.* **67,** 1778–1788 Medline
39. Luo, H., Broux, B., Wang, X., Hu, Y., Ghannam, S., Jin, W., Larochelle, C., Prat, A., and Wu, J. (2016) EphrinB1 and EphrinB2 regulate T cell chemotaxis and migration in experimental autoimmune encephalomyelitis and multiple sclerosis. *Neurobiol. Dis.* **91,** 292–306 CrossRef Medline
40. Tanaka, M., Kamata, R., Yanagihara, K., and Sakai, R. (2010) Suppression of gastric cancer dissemination by ephrin-B1-derived peptide. *Cancer Sci.* **101,** 87–93 CrossRef Medline
41. Gasman, S., Chasserot-Golaz, S., Popoff, M. R., Aunis, D., and Bader, M. F. (1997) Trimeric G proteins control exocytosis in chromaffin cells: Go regulates the peripheral actin network and catecholamine secretion by a mechanism involving the small GTP-binding protein Rho. *J. Biol. Chem.* **272,** 20564–20571 CrossRef Medline
42. Trifaro, J. M., Gasman, S., and Gutierrez, L. M. (2007) Cytoskeletal control of vesicle transport and exocytosis in chromaffin cells. *Acta Physiol. (Oxf)* **192,** 165–172 CrossRef
43. Gasman, S., Chasserot-Golaz, S., Bader, M. F., and Vitale, N. (2003) Regulation of exocytosis in adrenal chromaffin cells: focus on ARF and Rho GTPases. *Cell Signal.* **15,** 893–899 CrossRef Medline
44. Marjoram, R. J., Lessey, E. C., and Burridge, K. (2014) Regulation of RhoA activity by adhesion molecules and mechanotransduction. *Curr. Mol. Med.* **14,** 199–208 CrossRef Medline
45. Spiering, D., and Hodgson, L. (2011) Dynamics of the Rho-family small GTPases in actin regulation and motility. *Cell Adh. Migr.* **5,** 170–180 CrossRef Medline
46. Niggli, V., and Rossy, J. (2008) Ezrin/radixin/moesin: versatile controllers of signaling molecules and of the cortical cytoskeleton. *Int. J. Biochem. Cell Biol.* **40,** 344–349 CrossRef Medline
47. Okamoto, K., Bosch, M., and Hayashi, Y. (2009) The roles of CaMKII and F-actin in the structural plasticity of dendritic spines: a potential molecular identity of a synaptic tag? *Physiology (Bethesda)* **24,** 357–366 CrossRef Medline
48. Hung, R. J., Yazdani, U., Yoon, J., Wu, H., Yang, T., Gupta, N., Huang, Z., van Berkel, W. J., and Terman, J. R. (2010) Mical links semaphorins to F-actin disassembly. *Nature* **463,** 823–827 CrossRef Medline
49. Han, Y., Wang, X., Chen, J., and Sha, S. H. (2015) Noise-induced cochlear F-actin depolymerization is mediated via ROCK2/p-ERM signaling. *J. Neurochem.* **133,** 617–628 CrossRef Medline
50. Geneste, O., Copeland, J. W., and Treisman, R. (2002) LIM kinase and Diaphanous cooperate to regulate serum response factor and actin dynamics. *J. Cell Biol.* **157,** 831–838 CrossRef Medline
51. Vitale, M. L., Seward, E. P., and Trifaró, J. M. (1995) Chromaffin cell cortical actin network dynamics control the size of the release-ready vesicle pool and the initial rate of exocytosis. *Neuron* **14,** 353–363 CrossRef Medline
52. Gasman, S., Chasserot-Golaz, S., Malacombe, M., Way, M., and Bader, M. F. (2004) Regulated exocytosis in neuroendocrine cells: a role for subplasmalemmal Cdc42/N-WASP-induced actin filaments. *Mol. Biol. Cell* **15,** 520–531 CrossRef Medline
53. Sparrenberger, F., Cichelero, F. T., Ascoli, A. M., Fonseca, F. P., Weiss, G., Berwanger, O., Fuchs, S. C., Moreira, L. B., and Fuchs, F. D. (2009) Does psychosocial stress cause hypertension? a systematic review of observational studies. *J. Hum. Hypertens.* **23,** 12–19 CrossRef Medline
54. Liu, Y. Z., Wang, Y. X., and Jiang, C. L. (2017) Inflammation: the common pathway of stress-related diseases. *Front. Hum. Neurosci.* **11,** 316 CrossRef Medline
55. De Miguel, C., Rudemiller, N. P., Abais, J. M., and Mattson, D. L. (2015) Inflammation and hypertension: new understandings and potential therapeutic targets. *Curr. Hypertens. Rep.* **17,** 507 CrossRef Medline
56. Dominiak, P., and Grobecker, H. (1982) Elevated plasma catecholamines in young hypertensive and hyperkinetic patients: effect of pindolol. *Br. J. Clin. Pharmacol.* **13,** 381S–390S CrossRef Medline
57. Bühler, F. R., Amann, F. W., Bolli, P., Hulthén, L., Kiowski, W., Landmann, R., and Bürgisser, E. (1982) Elevated adrenaline and increased α-adrenoceptor-mediated vasoconstriction in essential hypertension. *J. Cardiovasc. Pharmacol.* **4,** S134–S138 CrossRef Medline
58. Borkowski, K. R., and Quinn, P. (1984) Adrenaline and the development of genetic hypertension. *J. Hypertens.* **2,** S81–83 Medline
59. Jablonskis, L. T., and Howe, P. R. (1994) Elevated plasma adrenaline in spontaneously hypertensive rats. *Blood Press* **3,** 106–111 CrossRef Medline
60. Axelrod, J. (1976) Catecholamines and hypertension. *Clin Sci Mol Med Suppl.* **3,** 415s–421s CrossRef Medline
61. Goldstein, D. S. (1983) Arterial baroreflex sensitivity, plasma catecholamines, and pressor responsiveness in essential hypertension. *Circulation* **68,** 234–240 CrossRef Medline
62. Byrne, C. J., Khurana, S., Kumar, A., and Tai, T. C. (2018) Inflammatory signaling in hypertension: regulation of adrenal catecholamine biosynthesis. *Front. Endocrinol. (Lausanne)* **9,** 343 CrossRef
63. Esler, M., Eikelis, N., Schlaich, M., Lambert, G., Alvarenga, M., Kaye, D., El-Osta, A., Guo, L., Barton, D., Pier, C., Brenchley, C., Dawood, T., Jennings, G., and Lambert, E. (2008) Human sympathetic nerve biology: parallel influences of stress and epigenetics in essential hypertension and panic disorder. *Ann. N.Y. Acad. Sci.* **1148,** 338–348 CrossRef Medline
64. Pende, A., Musso, N. R., Vergassola, C., Puppo, F., Ioverno, A., Criscuolo, D., Indiveri, F., and Lotti, G. (1990) Neuroendocrine effects of interferon α2A in healthy human subjects. *J. Biol. Regul. Homeost. Agents* **4,** 67–72 Medline
65. Corssmit, E. P., Heijligenberg, R., Endert, E., Ackermans, M. T., Sauerwein, H. P., and Romijn, J. A. (1996) Endocrine and metabolic effects of interferon-α in humans. *J. Clin. Endocrinol. Metab.* **81,** 3265–3269 CrossRef Medline
66. Kannan, H., Tanaka, Y., Kunitake, T., Ueta, Y., Hayashida, Y., and Yamashita, H. (1996) Activation of sympathetic outflow by recombinant human interleukin-1β in conscious rats. *Am. J. Physiol.* **270,** R479–R485 Medline
67. Rivier, C., Vale, W., and Brown, M. (1989) In the rat, interleukin-1α and -β stimulate adrenocorticotropin and catecholamine release. *Endocrinology* **125,** 3096–3102 CrossRef Medline
68. Mathar, I., Vennekens, R., Meissner, M., Kees, F., Van der Mieren, G., Camacho Londoño, J. E., Uhl, S., Voets, T., Hummel, B., van den Bergh, A., Herijgers, P., Nilius, B., Flockerzi, V., Schweda, F., and Freichel, M. (2010) Increased catecholamine secretion contributes to hypertension in TRPM4-deficient mice. *J. Clin. Invest.* **120,** 3267–3279 CrossRef Medline
69. Luo, H., Yu, G., Tremblay, J., and Wu, J. (2004) EphB6-null mutation results in compromised T cell function. *J. Clin. Investig.* **114,** 1762–1773 CrossRef Medline
70. Ory, S., Ceridono, M., Momboisse, F., Houy, S., Chasserot-Golaz, S., Heintz, D., Calco, V., Haeberlé, A. M., Espinoza, F. A., Sims, P. J., Bailly, Y., Bader, M. F., and Gasman, S. (2013) Phospholipid scramblase-1-induced lipid reorganization regulates compensatory endocytosis in neuroendocrine cells. *J. Neurosci.* **33,** 3545–3556 CrossRef Medline
71. Poëa-Guyon, S., Ammar, M. R., Erard, M., Amar, M., Moreau, A. W., Fossier, P., Gleize, V., Vitale, N., and Morel, N. (2013) The V-ATPase membrane domain is a sensor of granular pH that controls the exocytotic machinery. *J. Cell Biol.* **203,** 283–298 CrossRef Medline

72. Mosharov, E. V., and Sulzer, D. (2005) Analysis of exocytotic events recorded by amperometry. *Nat. Methods* **2,** 651–658 CrossRef Medline
73. Kolski-Andreaco, A., Cai, H., Currle, D. S., Chandy, K. G., and Chow, R. H. (2007) Mouse adrenal chromaffin cell isolation. *J. Vis. Exp.* **2,** 129 Medline
74. Sala, F., Nistri, A., and Criado, M. (2008) Nicotinic acetylcholine receptors of adrenal chromaffin cells. *Acta Physiol. (Oxf.)* **192,** 203–212 Medline
75. Martinez-Espinosa, P. L., Yang, C., Gonzalez-Perez, V., Xia, X. M., and Lingle, C. J. (2014) Knockout of the BK β2 subunit abolishes inactivation of BK currents in mouse adrenal chromaffin cells and results in slow-wave burst activity. *J. Gen. Physiol.* **144,** 275–295 CrossRef Medline
76. Solaro, C. R., Prakriya, M., Ding, J. P., and Lingle, C. J. (1995) Inactivating and noninactivating Ca^{2+}- and voltage-dependent K^+ current in rat adrenal chromaffin cells. *J. Neurosci.* **15,** 6110–6123 CrossRef Medline
77. Han, D. H., Chae, M. R., Jung, J. H., So, I., Park, J. K., and Lee, S. W. (2008) Effect of testosterone on potassium channel opening in human corporal smooth muscle cells. *J. Sex. Med.* **5,** 822–832 CrossRef Medline
78. Couchonnal, L. F., and Anderson, M. E. (2008) The role of calmodulin kinase II in myocardial physiology and disease. *Physiology (Bethesda)* **23,** 151–159 Medline
79. Menezes, A., Zeman, R., and Sabban, E. (1996) Involvement of intracellular or extracellular calcium in activation of tyrosine hydroxylase gene expression in PC12 cells. *J. Neurochem.* **67,** 2316–2324 Medline
80. Ginnan, R., Zou, X., Pfleiderer, P. J., Mercure, M. Z., Barroso, M., and Singer, H. A. (2013) Vascular smooth muscle cell motility is mediated by a physical and functional interaction of Ca^{2+}/calmodulin-dependent protein kinase IIdelta2 and Fyn. *J. Biol. Chem.* **288,** 29703–29712 CrossRef Medline